Pyrolytic Graphite And Carbon-Carbon Sputter Behaviour Under Xenon Ion Incidence

IEPC 2005-143

Presented at the 29th International Electric Propulsion Conference, Princeton University, October 31 – November 4, 2005

Michael Tartz*, Horst Neumann†
Leibniz-Institute for Surface Modification, Leipzig, Germany

Hans Leiter‡
EADS Space Technology, Möckmühl, Germany

Joachim Esch§
Schunk Kohlenstofftechnik, Heuchelheim, Germany

We performed angle and energy dependent sputter yield measurements of various prospective carbon ion thruster grid materials under xenon ion incidence in the energy range 200..1400eV and at normal and oblique incidence up to 70°. Materials investigated are high-dense graphite of various grain sizes, Carbon-Carbon material and pyrolytic graphite. No significant difference between the various carbon materials with respect to sputter yield was found.

I. Introduction

The sputter yield is a physical material parameter, which is important in lifetime investigations of components that are exposed to energetic ions. In gridded ion thrusters, grid eroding processes always take place leading to a gradually damage of the grids and, consequently, a limited lifetime of the thruster. In addition to the primary ions neutrals can escape from the plasma chamber, providing a neutral density within the grid system. Additionally, neutrals from the residual gas in the vacuum chamber may add to this neutral density. In a charge-exchange process, a primary ion collides with a neutral, converting the ion into a neutral and the former neutral into a slow ion. If this ion is born within the grid system or in its very vicinity, it may be accelerated towards one of the grids (cp. figure 1). Because of the gained energy, the ion impact will sputter some material from the grid. A detailed investigation showed that most of the charge-exchange ions impinge on the hole inside of the negatively biased accelerator grid, thus widening the holes during the operation[1]. Therefore, the hole evolution of the accelerator grid is most critical for the thruster lifetime.

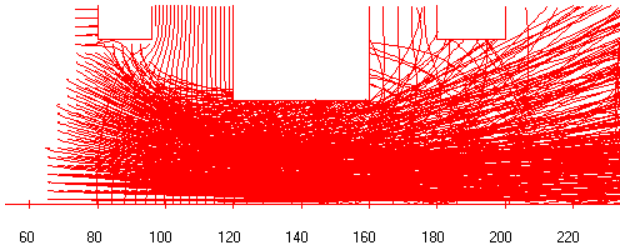

Figure 1: Trajectories of charge-exchange ions in a three-grid system simulated with IOM grid erosion code.

Since the sputter yield of the grid material determines the erosion rate and, hence, the grid lifetime, it is indispensable to determine the sputter yield in dependence on the energy and angle of incidence for promising grid materials. The obtained sputter

* michael.tartz@iom-leipzig.de
† horst.Neumann@iom-leipzig.de
‡ hans.leiter@space.eads.net
§ joachim.esch@schunk-group.com

characteristics allow to assess the applicability of the respective grid material. Furthermore, on the basis of these data, grid erosion simulation can predict reliable erosion rate and lifetime values.

Commonly, carbon and molybdenum are preferred as grid material. Molybdenum is state-of-the-art material despite of the rather high sputter yield. Carbon is widely used because of its low sputter yield, low density and low thermal expansion coefficient. Because of the good mechanical and thermal properties the carbon-carbon composite material (CC) increasingly becomes important for ion thruster grid systems. Furthermore, pyrolytic graphite (PG) came into the focus. Recently very low sputter yields of PG and CC were reported [2].

In a recent report [3] we presented sputter yield measurements of pure and modified molybdenum and titanium under xenon ion impact. Semi-empirical sputter yield models were found to describe the experimental data very well. The implantation of nitrogen into metals was proven to reduce the sputter yield because of the reduction of the reduced mass. A decrease of the sputter yield up to 40% was reported earlier by Wilbur [4]. We found a reduction of the molybdenum sputter yield by 10% and the titanium sputter yield by about 20% due to nitrogen implantation, however the achieved nitrided layers were too thin to make this effect applicable for prolongation of ion thruster grid lifetime.

Unfortunately, up to now only sparse sputter data are available for xenon incident on carbon materials. Generally, there is largely a lack of angular dependent sputter data.

This paper reports on sputter yield measurements for low energetic (≤1.5 keV) xenon ion impact on various kinds of high-density graphite, pyrolytic graphite and Carbon-Carbon material. The effect of the surface structures is studied. Special attention is paid to the long-duration sputter behavior. This work was performed within the “New Grid Systems for Ion Engines" Technology Project [5].

II. Experimental Setup

The sputter behaviour is investigated in a dedicated UHV chamber at IOM (figure 2), which is evacuated by a turbo pump (2000 l/s) to a background pressure of less than 10^{-8} mbar. As a result of the xenon gas flow through the sputter ion source the process pressure increases up to $5*10^{-5}$ mbar. The residual gas composition is permanently controlled by a quadrupole mass spectrometer. Typical spectra in figure 4 show that beside of the operation gas xenon only very low contents of water (about 6 orders of magnitude lower than xenon) and nitrogen are found in the chamber, pure oxygen was not detected. This ensures that additional chemical etching particularly on carbon in presence of oxygen practically not occurs. Sputter yield measurements of materials as titanium may be affected by a large amount of residual gas like nitrogen and oxygen due to the strong gettering effect, which falsifies

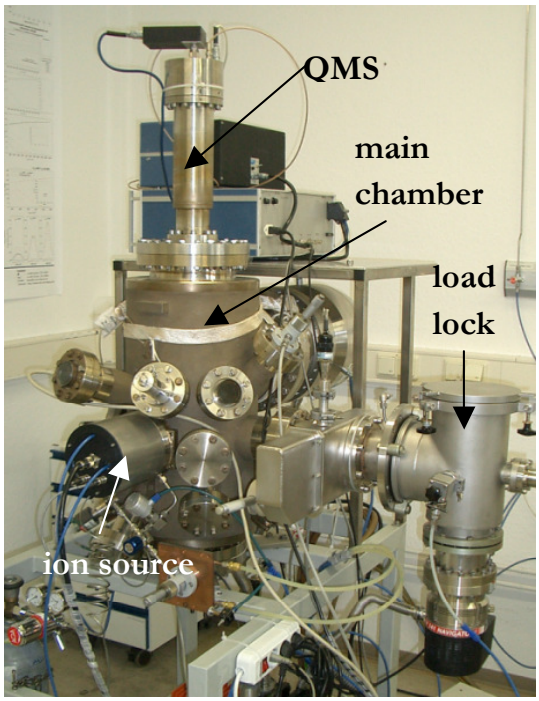

Figure 2: The IOM sputter test facility with load-lock, rf ion source and quadrupole mass spectrometer for residual gas analysis.

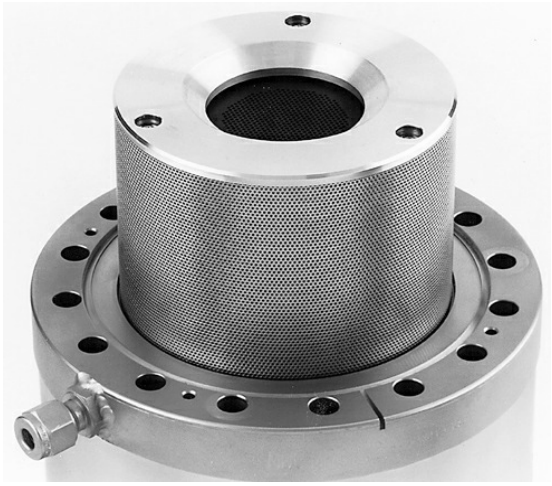

Figure 3: IOM radio-frequency ion beam source ISQ40.

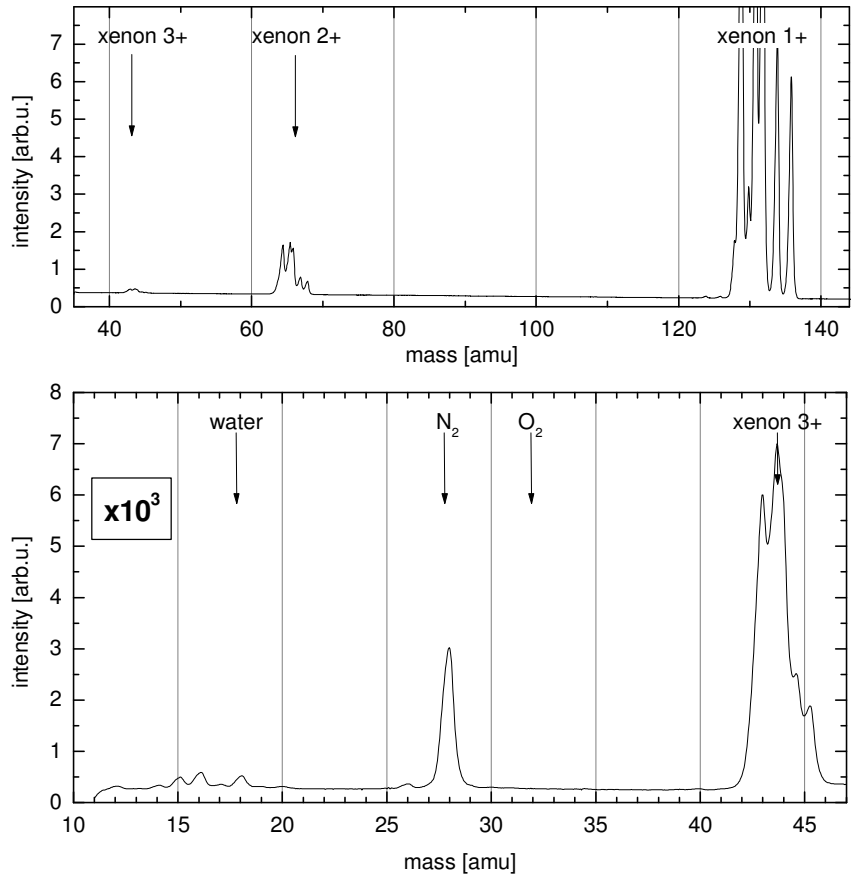

Figure 4: Residual gas spectra recorded by the quadrupole spectrometer not corrected for the mass detection efficiency function of the QMS. The content of residual gas is very low, the number of multiply charged ions is sufficiently small.

the sputter result. This can also be precluded here which has been proven experimentally.

The samples are transferred into the vacuum chamber by a load-lock chamber, therefore keeping the extraordinary vacuum in the test facility.

The xenon ion beam is produced by an ISQ 40 RF ion source (figure 3) as developed at IOM [6]. The initial beam diameter is 3 cm. A low divergence two-grid extraction system is used to apply a high ion current density up to 3 mA/cm^2 on the target. The source operates at ion energies between 50 and 2000 eV. The source can operate with almost all gases, for these measurements xenon gas is feed by a mass flow controller.

The sputter targets are placed in the beam centre at a distance of 12 cm from the grids. The targets can be tilted against the beam direction. The target current is directly measured and logged by a computer. The samples are weighed before and after sputtering employing a high-precision microbalance with a precision of 10 µg. The sputter time had to be chosen large enough to obtain a reliable detectable mass difference. The sputter yield is estimated from the weight loss and the target current corrected by the charge-exchange ions which contribute to the sputtering process but not to the current measurement [7].

Because the surface roughness may influence the sputter yield the sample surface structure of selected samples is studied by scanning electron microscopy.

The samples were prepared from the respective material as it was delivered. No surface treatment has been made before sputtering. In order to study the effect of the surface topography on the sputter yield, some samples were mechanically polished.

III. Model of sputter yield

There are semi-empirical descriptions of the sputter yield in dependence on ion energy and incidence angle. In our grid erosion simulation we use a revised version of the well-known Bohdansky formula [8]

$$Y(E,\alpha=0°) = Q\ s_n(\varepsilon)\left(1-\left(\frac{E_{th}}{E}\right)^{2/3}\right)\left(1-\frac{E_{th}}{E}\right)^2$$

where ε and s_n are the reduced energy and the nuclear stopping cross section, respectively,

$$\varepsilon = E(eV)\frac{M_2}{M_1+M_2}\ \frac{0.03255}{Z_1Z_2\left(Z_1^{2/3}+Z_2^{2/3}\right)^{1/2}}$$

$$s_n(\varepsilon) = \frac{0.5\ln(1+1.2288\varepsilon)}{\varepsilon+0.1728\sqrt{\varepsilon}+0.008\varepsilon^{0.1504}}.$$

Z_1 and Z_2 are nucleus charge numbers, M_1 and M_2 are mass numbers of projectile and target. Q is a scale factor and E_{th} is the sputtering threshold energy, both are used as fitting parameters.

The angular dependence of the sputter yield is given by the Yamamura model [9] which describes the sputter yield as an angular dependent factor to the yield $Y(\alpha=0°,E)$ at normal incidence

$$\frac{Y(\alpha,E)}{Y(0°,E)} = (\cos\alpha)^{-f}\ \exp\left[f\left(1-(\cos\alpha)^{-1}\right)\cos\alpha_{opt}\right]$$

Here α_{opt} is the incidence angle at which maximum sputtering occurs, f is a fit parameter. Yamamura *et al* gave empirical formulae for the parameters α_{opt} and f, basing on a large number of experimental sputter data of various projectile-target-combinations. Parameter f is approximated by

$$f = f_{sig}\left(1+2.5\frac{\zeta}{1-\zeta}\right)$$

with $\zeta = \sqrt{\frac{E_{th}}{E}}$ and a fitting parameter f_{sig}. The optimum incidence angle is given by

$$\alpha_{opt} = 90° - 286.0\left(\frac{p}{\sqrt{E(keV)}}\right)^{0.45},$$

with p as another parameter.

Particularly in the case of heavy ion sputtering the description reveals a singular behavior at threshold energy which is overcome by an interpolation.

The parameters Q, E_{th}, f_{sig} and p can be taken from the literature data collections [9,10]. However, in some cases, particularly for the ion-target combinations considered here, the supply of experimental data is quite poor and the literature parameters yield insufficient descriptions of the sputter yield. In that cases, the parameters have to be determined from fits to the experimental data. Table 1 in the summary section gives the parameter values which were actually used in the simulation in this study.

IV. Results and Discussion

Figure 5 shows the energy and incidence angle dependent sputter yields of graphite, CC and pyrolytic graphite. No significant difference between the various carbon materials with respect to sputter yield can be observed. The sputter yield of pyrolytic graphite seems to be slightly lowered compared to the others by a few percent, which is just at the edge of the measurement error.

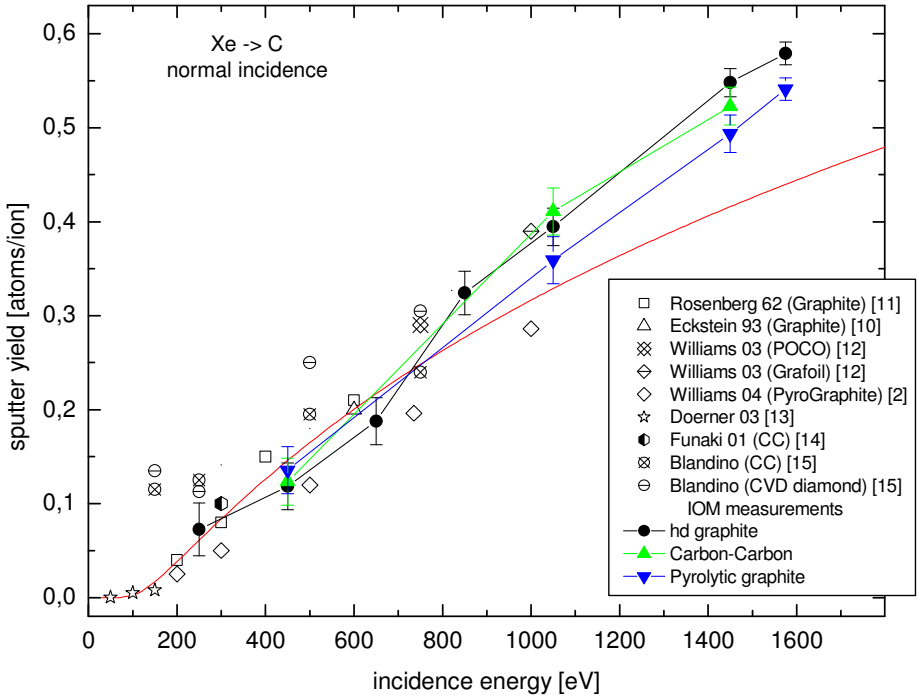

Figure 5: Energy dependent sputter yield of carbon materials. The solid lines are the simulated sputter yields.

The data agree well with other published data and with the sputter model. It seems that the simulation underpredicts the sputter yields at higher energies. This is also true at higher ion energies where the few published data clearly follow the trend given by these low-energy data; here the simulation results are much to low. The fitting of the model yielded a significant change of the parameters (see table 1) because the literature parameter gave too-low sputter yields.

Figure 6 shows the angular dependent sputter yield results of the carbon materials. For small incidence angles no differences between the various carbon types can be seen as in the normal-incidence data. However, for larger incidence angles the materials separate, the pyrolytic graphite sputter yield is lower than that of CC and that of high-density graphite for all incidence energies considered here. This is probably an effect of the sample surfaces and is discussed later.

The sputter yield model by Yamamura gives a good agreement with the experimental data. The underprediction of the energy dependent model at higher energies as mentioned above leads also to lower modeled sputter yields here; normalizing e.g. the normal incidence model data at 1400eV to the respective experimental value gives an excellent agreement with measured angular data.

It is obvious and well known that the surface topology will have an huge effect on the sputter yield, particularly the angular dependent sputter yield strongly depends on the surface. For a rough surface an increased normal incident sputter yield will be observed as compared to a flat surface. With increasing incidence angle the actual ion incidence angles will not change so much at a rough surface than at a flat surface, consequently the rough surface sputter yield increases less than that of the flat surface. In particular configurations the sputter yield may stay constant or decrease with growing incidence angle. In the proceeding surface erosion an equilibrium surface topology evolves which usually differs from the initial surface topology. Consequently, the sputter yield measured will change with the sputter time when the surface changes to the stable topology. This lays particular emphasis on the measuring sputter time. As example, measuring the sputter yield by the mass change of a deposited layer on a QCM can be done at very short sputter times due to the high sensitivity of the QCM. However, only a few atomic layers were removed and the surface of the sample could not change very much in that time, therefore the determined sputter yield is that of the initial surface. In contrast, measuring the mass loss conventionally as we have done here requires larger sputter times, which removes significant depth of material. Usually, the surface has changed in that time and may have

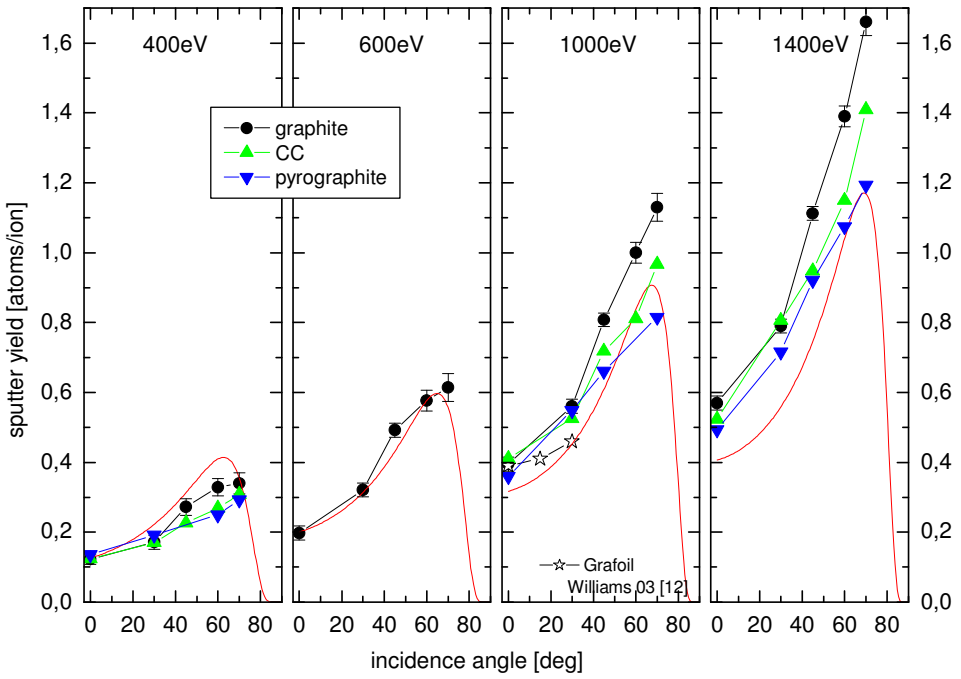

Figure 6: Energy and incidence angle dependent sputter yield of carbon materials. The solid lines are the simulated sputter yields.

reached the equilibrium state; therefore the measured sputter yield is largely determined by the dynamically later surface state and very little by the initial state.

In order to prove these effects of the surface, some samples were polished by very fine abrasive paper and investigated by SEM after the sputtering at normal incidence. Figure 7 shows the change in the surface topology of high-density graphite samples due to sputtering. However, no significant difference in sputter yield could be detected between a polished and unpolished surface after some hours of sputtering. It is therefore concluded that in both cases a similar surface topography evolves (cf. figure 7, bottom) which remains stable for a long sputter time. If the samples would be sputtered in shorter time one could expect an effect of the polished surface, but such measurements cannot be performed currently because of the minimum required mass difference and the small sample sizes. On the other hand, keeping in mind the application as thruster grid material or other long-duration use, the starting surface will clearly not have a significant effect on the lifetime.

Figure 8 shows the change in surface structures of graphite samples with different grain sizes. Here, also no significant difference in sputter yield could be found, indicating that the grain size has negligible effect on the sputter yield. The resulting stable surfaces are very similar.

Figure 9 shows SEM figures of the surface of PG before and after sputtering at normal incidence. The pyrolytic graphite has a much closer surface compared to the sponge-like graphite surface. The density is somewhat larger than that of high-density graphite. As mentioned above, a slightly lower sputter yield of pyrolytic graphite compared to the high-density graphite was found which is probably the result of the rather smooth PG surface, but which is not very significant because of the experimental error. The PG surface became somewhat smoother after sputtering.

Carbon-Carbon material has a regular surface topology consisting of layers of fibers (cf. figure 10), which leads at normal incidence to a distribution of the actual incidence angles up to 90° with a medium angle of 47°. An earlier study resulted in a CC sputter yield larger by a factor of 2 compared to that of graphite [16] which could be readily explained by the surface topology. However, the results of this study differ from the older findings where the measuring time, i.e. the material removal was lower.

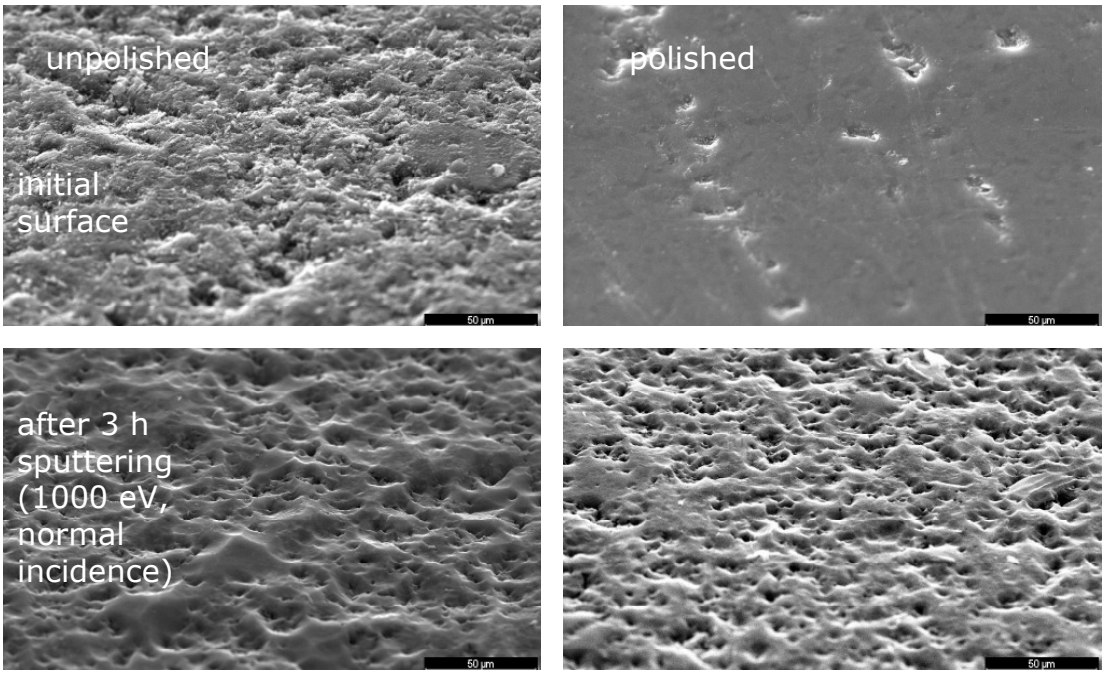

Figure 7: SEM figures of the high-density graphite surface before and after sputtering. left: untreated initial surface, right: polished initial surface.

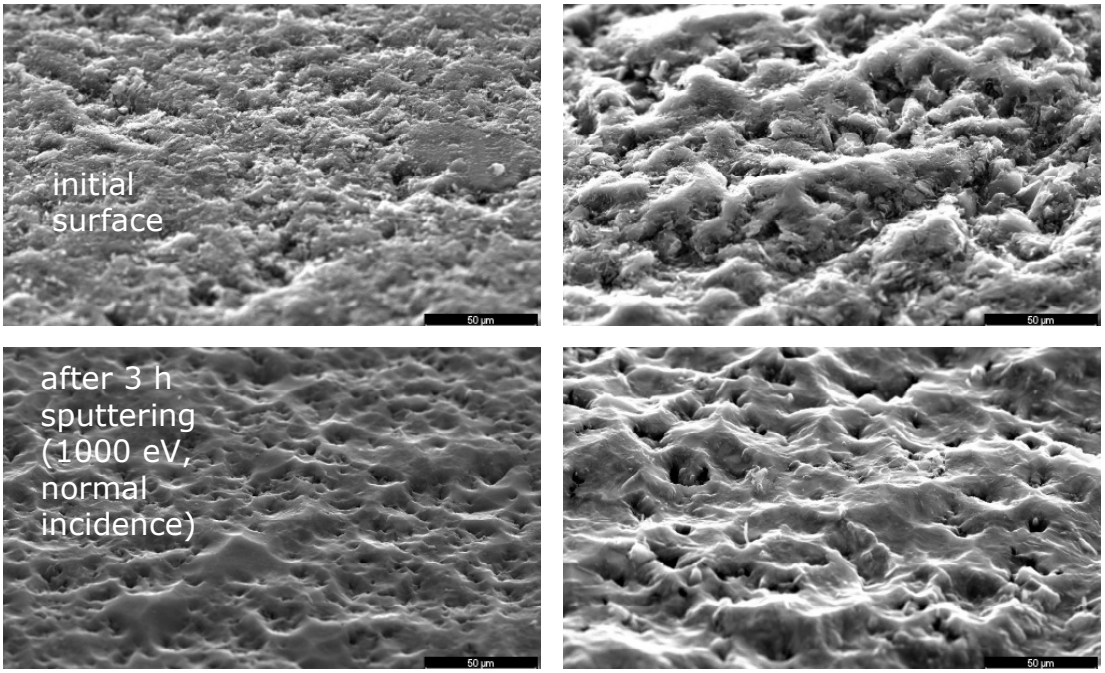

Figure 8: SEM figures of the graphite surfaces of different grain sizes: left: 2 µm, right: 30 µm.

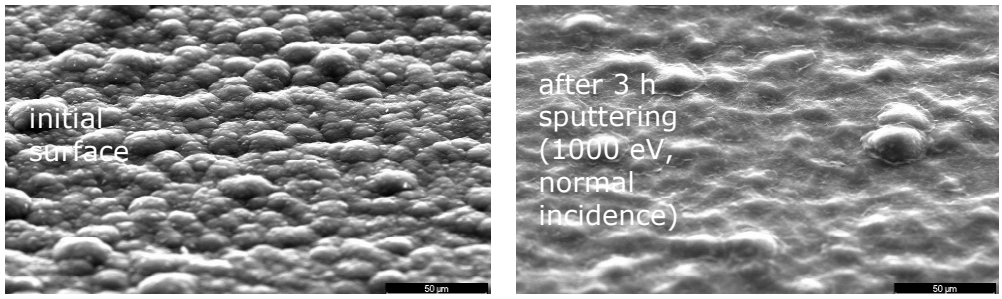

Figure 9: SEM figures of pyrolytic graphite before and after sputtering.

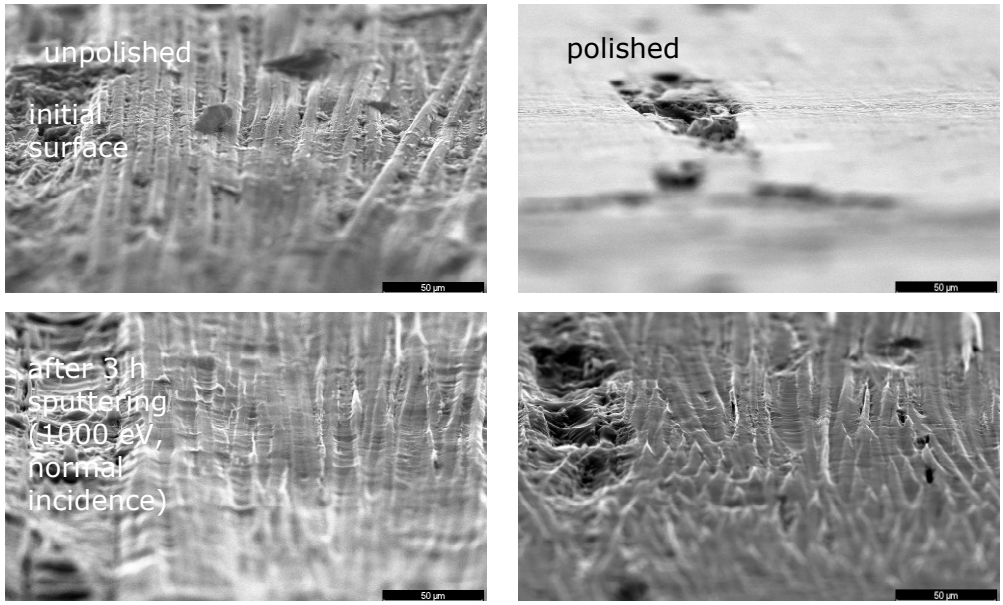

Figure 10: SEM figures of Carbon-Carbon material before and after sputtering, right: initial polished surface.

In order to visualize the effect of the CC surface topography on the sputter yield CC samples were polished. Figure 10 (right) shows SEM figures of the surface before and after 3h sputtering. It is obvious that after sputtering the surfaces evolved to similar structures. The sputter yield at 1000eV of the unpolished sample was found to be slightly higher (0.43) as for the polished sample (0.39). Continuing the sputtering on both samples the yields approaches the value of graphite (0.39). The large scattering of sputter data for CC is currently not understood.

V. Conclusion

Sputter yields have been measured for various carbon materials in dependence on ion energy and incidence angle in the incidence parameter range of interest for ion thrusters. The data was found in good agreement with other published data if available.

With respect to the experimental error no difference between high-density graphite, CC and pyrolytic graphite could be found. The large sputter yield advantage of CC and pyrolytic graphite over graphite as recently reported could not be verified here. This makes Carbon-Carbon anyway an excellent grid material for long-life applications.

The simulation of the sputter yield was found to describe the experimental data in good agreement. Table 1 summarises the fitting parameters used in the modeling of sputter yield (cf. section 3). The parameters have been slightly adapted to fit the sputter model to the experimental results. Please note that the parameters in table 1 do not necessarily have a clear physical meaning.

Table 1: Fitting parameter used in the simulation of the carbon sputter yield (cf. chapter 3)

E_{th}	70
Q	4.61
f_{sig}	1.7
p	0.11

Acknowledgments

Financial support by the European Space Agency via the “New Grid Systems for Ion Engines" Technology Project is gratefully acknowledged.

References

[1] M. Tartz, E. Hartmann, H. Neumann, *Evolution of extraction grid erosion with operation time*, AIAA-2004-3787, 40th Joint Propulsion Conference, Fort Lauderdale, FL, July 11-14, 2004.

[2] J. Williams, M. Johnson and D. Williams, *Differential Sputtering Behavior of Pyrolytic Graphite and Carbon-Carbon Composite Under Xenon Bombardment*, AIAA-2004-3788, 40th Joint Propulsion Conference, Fort Lauderdale, FL, July 11-14, 2004.

[3] M. Tartz, D. Manova, H. Neumann, H. Leiter, J. Esch, *Sputter investigation of ion thruster grid materials*, Paper Nr. AIAA-2005-4414, 41. Joint Propulsion Conference, Tucson, AZ, 10.-13.07. (2005).

[4] P. Wilbur, J. Miller, D. Williamson, *Effects of ion implanted C and N on the sputter behaviour of Ti and Mo grid materials*, IEPC paper IEPC-01_117, 27th Int. Electric Propulsion Conf. , Pasadena, Oct 2001.

[5] H. Leiter *et.al.*, The "New Grid Systems for Ion Engines" Technology Project - Results and Conclusions, IEPC 2005-132, 29th Int. Electric Propulsion Conf., 31.10.-4.11.2005, Princeton.

[6] M. Zeuner, F. Scholze, B. Dathe, H. Neumann, *Optimisation and characterisation of a TCP type RF broad beam ion source*, Surf. Coat. Tech. 142-144 (2001) 39-48.

[7] M. Tartz, E. Hartmann, F. Scholze, H. Neumann, F. Bigl, *A new approach to ion beam modelling*, Surf. Coat. Technol. 97 (1997) 504.

[8] C. Garcia-Rosales, W. Eckstein, J. Roth, *Revised formulae for sputtering data*, J. Nucl. Mat. 218 (1994) 8.

[9] Y. Yamamura, Y. Itikawa, N. Itoh, *Angular dependence of sputtering yields of monatomic solids*, Institute of Plasma Physics, Nagoya University, Report IPPJ-AM-26.

[10] W. Eckstein, C. Garcia-Rosales, J. Roth, W. Ottenberger, *Sputtering data*, Max-Planck-Institut für Plasmaphysik Report IPP 9/82 (1993).

[11] D. Rosenberg, G. K. Wehner., J. Appl. Phys. 33 (1962) 1842.

[12] J. Williams, M. Gardner, P. Wilbur, *Xenon sputter yield measurements for ion thruster materials*, IEPS paper IEPC-03-130, 28th Int. Electric Propulsion Conf. , Toulouse, 17.-21. March 2003.

[13] R. Doerner, D. Goebel, *Sputtering yields of ion thruster grid and cathode materials during low energy xenon plasma bombardment*, AIAA paper AIAA-2003-4561, 39th Joint Propulsion Conf., Huntsville, AL, 20.-23. July 2003.

[14] I. Funaki et al, *20mN-class Microwave Discharge Ion Thruster*, Paper IEPC-01-103, 27th Int. Electric Propulsion Conf, Pasadena, 15-19 October 2001.

[15] J. J. Blandino, D. G. Goodwin, C. E. Garner, AIAA 96-3203, 32. JPC, 1996.

[16] R. Deltschew, M. Tartz, V. Plicht, E. Hartmann, H. Neumann, H.J. Leiter, J. Esch, *Sputter characteristics of carbon-carbon compound material*, Paper IEPC-01-118, 27th Int. Electric Propulsion Conf., Pasadena, CA, 15-19 October, 2001.